Highlights

1. A new comprehensive six degrees-of-freedom lump mass model of drill-string suitable for horizontal wells was proposed.
2. The models aims to investigate instabilities caused by cutting rock formations and frictional effects within a Bottom Whole Assemble (BHA) and a drill-string.
3. We have observed all types nonlinear effects including stick-slip, bit bounce and whirling.

Graphical Abstract

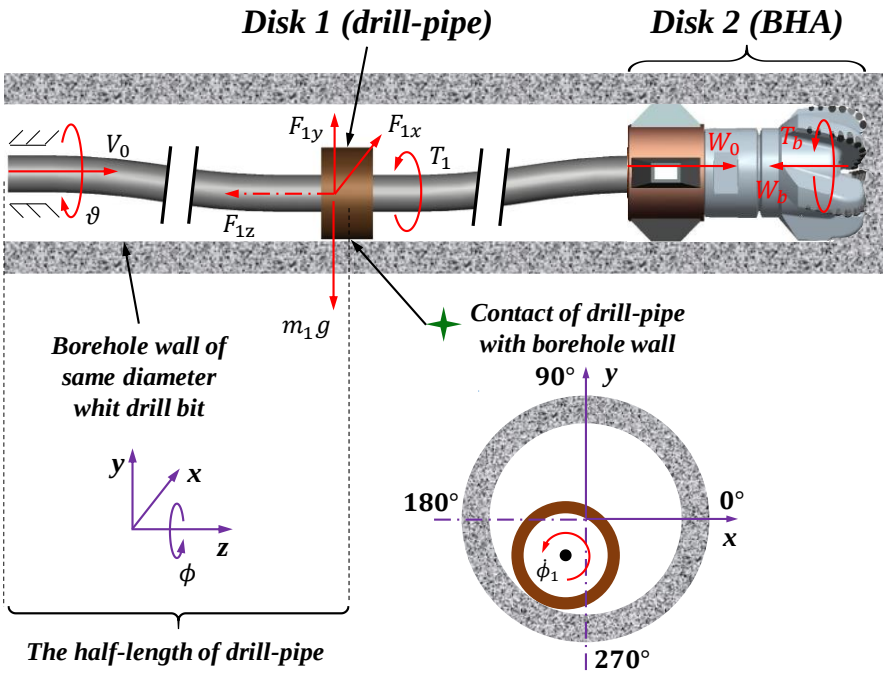

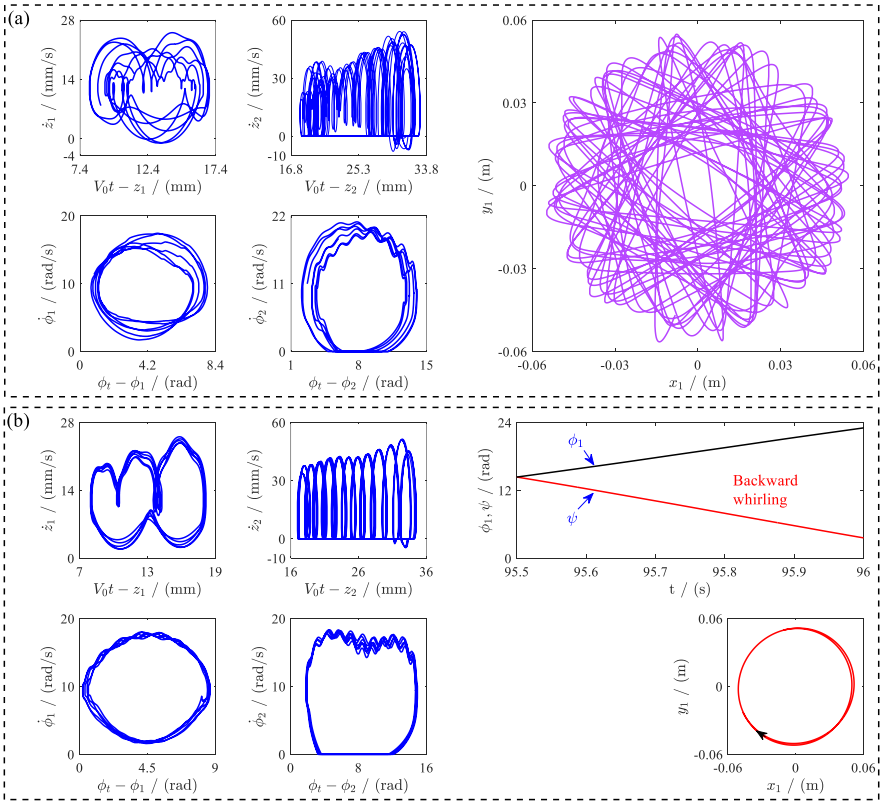

Nonlinear dynamics of lump mass model of drill-string in horizontal well

Dou Xie[a,b], Zhiqiang Huang[a,*], Yachao Ma[a], Vahid Vaziri[b], Marcin Kapitaniak[b], Marian Wiercigroch[b]

[a] *School of Mechatronic Engineering, Southwest Petroleum University, Chengdu, Sichuan 610500, PR China*
[b] *Centre for Applied Dynamics Research, School of Engineering, University of Aberdeen, Aberdeen AB24 3UE, UK*

Abstract

We develop a dynamic model of a drill-string in a horizontal well having six degrees-of-freedom, which accounts for longitudinal, lateral and torsional motions. In this model, nonlinearities that arise due to intermittent contacts of a drill-pipe with a borehole wall and complex interactions between a drill-bit and a rock formation are all considered. The lateral motions of the drill-bit are restricted and its interactions with a borehole generate an interlaced force being result of a friction and a cutting that has a regenerative effect. In the cutting process, a state-dependent time delay is introduced to couple the axial and torsional motions of the drill-bit. The dynamic model established in this article is tested where the friction and cutting effects are gradually switched on, which shows that the model is robust. Subsequently, the complex whirling of a horizontal drill-string are analyzed and a particular attention is given to the influence of driving rotation speed and dynamic friction coefficient. The study should help us to better understand nonlinear dynamic effects of drill-strings in horizontal wells, which will lay a foundation for optimizing drilling parameters.

Keywords:

Horizontal well; Drill-string dynamics; Coupled motions; State-dependent delay; Complex whirling

1. Introduction

Horizontal wells drilled along oil and gas reservoirs may increase production by as much as seven times when compared to vertical ones as reported in [1]. Therefore, the horizontal well drilling technology is being developed rapidly allowing to reach reserves which may not be possible for conventional wells, for example see [2]. Horizontal drilling is complex and requires many specialized equipment and processes to be in place. A drill-string plays a key role, and as it is schematically shown in Fig. 1a, it is used to deliver a rotary motion applied at the surface and an axial force to a drill-bit. In general, a drill-

*Corresponding author.
Email addresses: xied_swpu@foxmail.com (Dou Xie), huangzq@swpu.edu.cn (Zhiqiang Huang), mayachao1206@163.com (Yachao Ma), vahid.vaziri@abdn.ac.uk (Vahid Vaziri), marcin.kapitaniak@abdn.ac.uk (Marcin Kapitaniak), m.wiercigroch@abdn.ac.uk (Marian Wiercigroch)

string is composed of many pipes connected through joints reaching a length even of several kilometers. A diameter of borehole is larger than that of a drill-pipe, and this results in an annulus space, which is primarily filled by drilling fluids. Such well configurations are prone to strong nonlinearities arising from a large deformation of a drill-string, its intermittent contacts with a borehole wall and complex interactions between a drill-bit and a drilled formation, as schematically depicted in Fig. 1b. These effects can generate dangerous dynamic phenomena including stick-slip, bit-bounce and whirling, which in turn are the root cause of wear and even catastrophic failures of drilling tools [4].

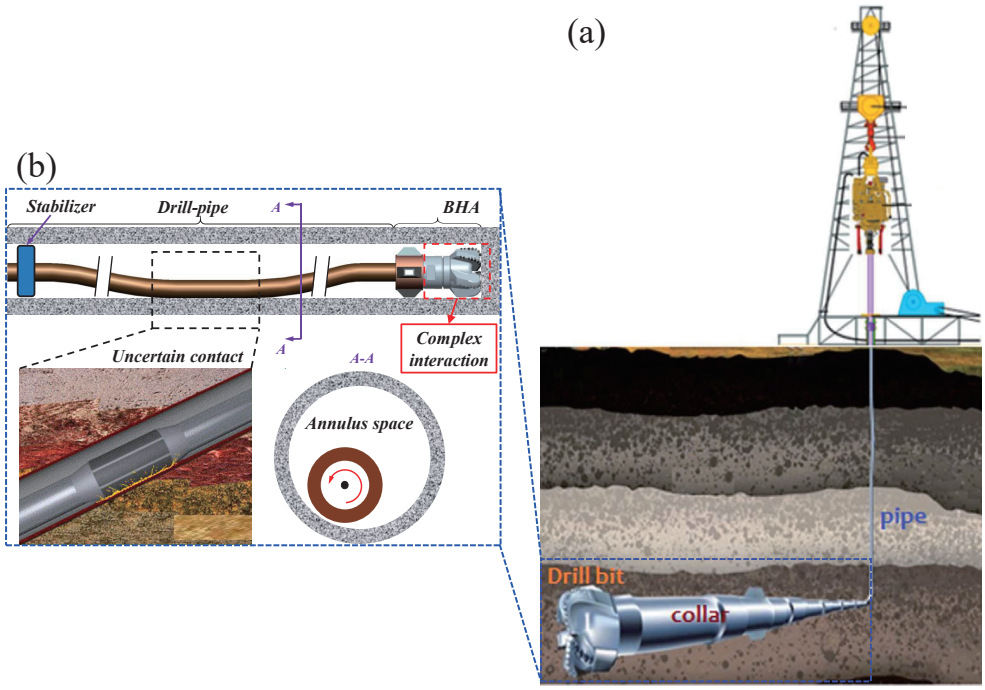

Figure 1: Schematics of (a) a typical rig used to drill horizontal wells adopted from [3], including main components of drill-string: drill-pipes and a Bottom Hole Assembly (BHA) comprised of a drill-bit and drill-collars; (b) a drill-string in a horizontal well showing main sources of nonlinearities.

For this reason, Measurement While Drilling (MWD) tools have been developed to gather downhole data and monitor vibration (see e.g. [5]), which in principle should provide some data for mathematical modelling and analysis of the complex dynamic interactions mentioned above. Especially in directional and horizontal drilling control, drilling dynamics play a vitally important role [6]. These problems have stimulated research in this area, most of which are dynamic analysis of longitudinal, torsional and lateral vibration of drill-strings in vertical wells (see e.g. [7, 8]). The interactions between a rotating drill-string and a borehole wall have also been researched in many works including [9–15]. In addition, vibration of a horizontal drill-string has attracted attentions of so many researchers, which will be briefly discussed next.

Tian *et al.* [16] conducted an experimental study of a drill-string to analyze its dynamic behaviour in a horizontal well, and developed a modeling approach to describe randomness of wellbore friction. Lian *et al.* [17] and Lin *et al.* [18] established an experimental rig to study the kinematic characteristics of a horizontal drill-string, and a particular attention was paid to its lateral vibration. Ritto *et al.* [19] proposed a dynamic model with stochastic frictional coefficient to study the axial and torsional motions of a horizontal drill-string, and introduced a simplified exponential model to describe the interaction between the drill-bit and rock. Cunha Jr. *et al.* [20] analyzed nonlinear dynamics of a drill-string in a horizontal well based on a beam theory, and considered interactions between a drill-bit and rock as a parametric probabilistic function. Wilson and Heisig [21] established a three-dimensional nonlinear dynamic model with fully coupled effects and studied the axial and lateral vibration of a drill-string in a horizontal well exhibiting friction induced vibration. Sarker *et al.* [3] proposed a bond graph dynamic model of a horizontal drill-string to predict its coupled longitudinal and torsional motions. Liu and Gao [22] established a dynamic model with 4 DOF to describe the dynamics of a drill-string in a deviated well, in which the stick-slip, lateral and torsional vibration of a drill-string and fluid damping effects were considered. Han *et al.* [23] established a nonlinear model of a drill-string in a horizontal well based on geometrically exact beam theory and quadrature element method, but just considered the geometric nonlinearity of a drill-string and its nonlinear contact with a borehole wall. As can be seen from this review, there is a lot of interest in modelling dynamics of drill-strings in horizontal wells, however we feel that some of the simplifications went too far. Specifically, the contact of a drill-pipe with a borehole wall, the interactions between a drill-bit and a drilled formation are over simplified and the couplings between axial, torsional and lateral vibration are largely neglected.

The aim of current work is to develop a simple drill-string dynamic model in a horizontal well accounting for all essential mechanisms and couplings, which are nonlinear. For this purpose, a new six degrees-of-freedom (6-DOF) model of a horizontal drill-string is developed in Sections 2 and 3, where both interactions of a drill-pipe with a borehole wall and a drill-bit with a rock formation are considered. In Section 4, the developed dynamic model is tested, where the effects of friction, cutting and regeneration are gradually switched on. Subsequently, whirling research of a horizontal drill-string is given in Section 5. Finally, some conclusions are drawn in Section 6.

2. Model description

The physical model of a drill-string in a horizontal well has two essential parts as shown in Fig. 1b: (i) a long pipe which is formed by many drill-pipes connected one to each other through screw threads,

and (ii) a BHA which is composed of drill collars, stabilizers and a drill-bit [24]. These two parts have different operational conditions, so their dynamic behaviour will be discussed separately. The geometry and physical parameters of the drill-string discussed here are given in Table 1. L_i, D_{i1} and D_{i2} are the respective length, outer and inner diameters, in which the subscript $i = p$ represents the drill-pipe and $i = c$ denotes the drill collar. D_b is the diameter of the drill-bit. E, G and ρ are the elasticity modulus, shear modulus and density of the drill-pipe, respectively.

Table 1: Typical geometry and physical parameters of a horizontal drill-string [25].

Parameter	Value	Unit	Parameter	Value	Unit
L_p	1000	m	L_c	200	m
D_{p1}	0.127	m	D_{c1}	0.152	m
D_{p2}	0.108	m	D_{c2}	0.057	m
D_b	0.216	m	E	200	GPa
ρ	8×10^3	kg/m^3	G	77	GPa

2.1. Model Simplifications

For an idealized drill-string under consideration, we assume: (i) the borehole is straight and its diameter is equal to that of the drill-bit, (ii) the damping effects of drilling fluid are neglected, and (iii) the lateral motions of the BHA and the left of the horizontal drill-string are restricted [16]. Based on these assumptions, a lumped mass model composed of two disks is proposed, as shown in Fig. 2. In this system, the inertial properties of the drill-pipe are represented by *Disk 1* and those of the BHA by *Disk 2*, and these two disks are linked to each other by means of an elastic shaft.

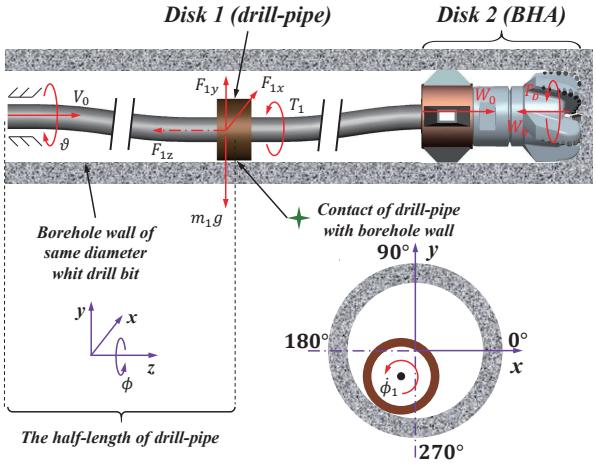

Figure 2: Physical model of a discrete drill-string in horizontal well section, where upper panel shows the lumped mass model of the drill-string and lower panel shows the contact of drill-pipe with borehole wall.

According to this physical model of the drill-string, the dynamics of *Disk 1* are described by 4 DOF,

one longitudinal, one torsional and the other two lateral. Because the lateral motions of the BHA are limited by a stabilizer, the dynamic properties of *Disk 2* are only described by 2 DOF for longitudinal and torsional motions. The system is driven from top by a constant axial velocity V_0 and a constant angular speed $\dot{\phi}_t = \vartheta$. Meanwhile, the effective weight on bit (WOB) W_0 acts as a control parameter and is directly applied on *Disk 2*.

2.2. Equations of motion

In order to establish the dynamical model, a coordinate system $(x - y - z - \phi)$, in which ϕ is the positive rotation direction about the z axial, was chosen. Hence, the spatial locations of *Disk 1* and *Disk 2* can be determined by coordinates $(x_1 - y_1 - z_1 - \phi_1)$ and $(z_2 - \phi_2)$, respectively. The contact between the drill-pipe and borehole wall is modeled as linear elastic, as illustrated in Fig. 3. To model the planar motion of the drill-pipe, a linear eccentricity e associated with *Disk 1* is introduced [9]. O_w and O_p are the geometric centres of the borehole and drill-pipe, respectively. β is the radial offset distance of O_p relative to O_w. υ is the radial clearance between the drill-pipe and borehole wall.

$$\beta = \sqrt{x_1^2 + y_1^2}, \quad \upsilon = (D_b - D_{p1})/2. \tag{1}$$

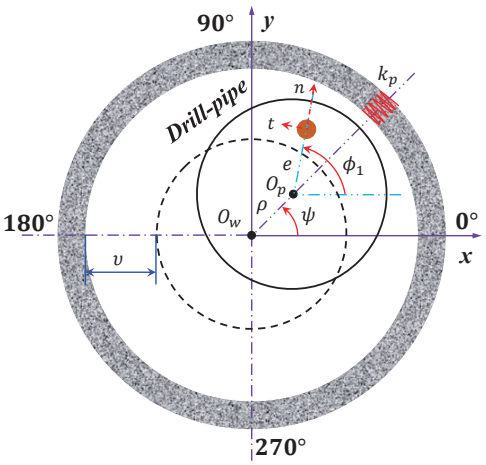

Figure 3: Schematic to model the lateral motions of drill-pipe, represented as drill-pipe rotating around its centroid O_p with velocity $\dot{\phi}_1$ inside the borehole of radial clearance υ.

By substituting the expressions for kinetic energy, potential energy and energy dissipation function given in Appendix A into the Lagrange equation, the equations to describe the motions of the horizontal drill-string system as shown in Fig. 2 can be written as Eq. (2), in which the values of the involved characteristic parameters are listed in Table 2.

$$
\begin{aligned}
&m_1\ddot{x}_1 + c_b\dot{x}_1 + k_b x_1 = F_{1x} + m_1 e\dot{\phi}_1^2 \cos\phi_1,\\
&m_1\ddot{y}_1 + c_b\dot{y}_1 + k_b y_1 = F_{1y} + m_1 e\dot{\phi}_1^2 \sin\phi_1 - m_1 g + F_u,\\
&m_1\ddot{z}_1 + c_a\dot{z}_1 + k_a\left(2z_1 - z_2 - V_0 t\right) = 0,\\
&J_1\ddot{\phi}_1 + c_t\dot{\phi}_1 + k_t\left(2\phi_1 - \phi_2 - \phi_t\right) = -T_1,\\
&m_2\ddot{z}_2 + c_a\dot{z}_2 + k_a\left(z_2 - z_1\right) = W_0 - W_b,\\
&J_2\ddot{\phi}_2 + c_t\dot{\phi}_2 + k_t\left(\phi_2 - \phi_1\right) = -T_b.
\end{aligned}
\tag{2}
$$

where k_a, k_b and k_t are the respective longitudinal, bending and torsional stiffness coefficient, and they are listed in Appendix A. F_{1x}, F_{1y} and T_1, which arise from the interaction between the drill-pipe and borehole wall, are the forces along x and y directions and torque acting on the drill-pipe, respectively. F_u is the buoyancy force acting on the drill-pipe generated from the effect of drilling fluid. W_b is the WOB and T_b is the torque on bit (TOB), which are caused by the interaction between the drill-bit and rock. Three damping coefficients are written in corresponding dimensionless forms as follow [26].

$$
\eta = \frac{c_a}{2\sqrt{k_a m_1}}, \quad \kappa = \frac{c_b}{2\sqrt{k_b m_1}}, \quad \xi = \frac{c_t}{2\sqrt{k_t J_1}}. \tag{3}
$$

Table 2: Typical parameters in the governing equations.

Parameter	Value	Unit	Parameter	Value	Unit
m_1	2.8×10^4	kg	k_b [8]	2.6×10^5	N/m
m_2	2.5×10^4	kg	k_t	938	Nm/rad
J_1	97.5	kgm^2	η	0.02	/
J_2	83	kgm^2	κ	0.02	/
e	8×10^{-3}	m	ξ	0.02	/
k_a	7×10^5	N/m	F_u	1.2×10^5	N

3. Contact scenarios

During a drilling process, essential nonlinearities of the drill-string dynamics primarily arise from intermittent contacts of a drill-pipe with a borehole wall and complex interactions between a drill-bit and a rock (see for example, [15], [26], [27]). To improve the predictive capabilities of our dynamic model, both of these two factors are modeled in this section.

3.1. Contact of a drill-pipe with a borehole wall

Contact conditions between a drill-pipe and a borehole wall depend on the motion state of the drill-pipe, so that we must establish a common model to simulate an intermittent contact. In general, the contact

force acting on a drill-pipe can be decomposed to two parts: a normal force F_n and a tangential force F_t arising due to friction, as shown in Fig. 4. In order to calculate the normal contact force, a penetration of a drill-pipe into borehole wall δ can be defined as

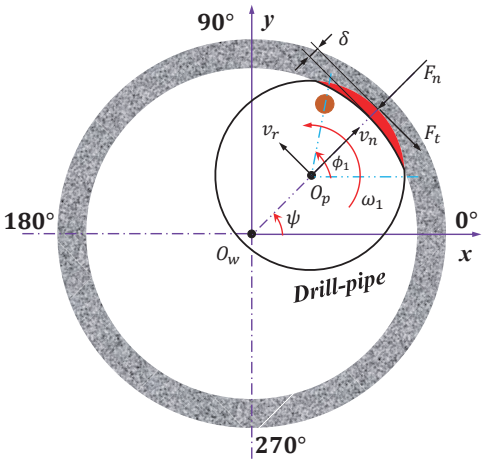

Figure 4: Schematic to model contact of a drill-pipe with a borehole wall, showing kinematics and forces generated when a drill- pipe penetrates into a borehole wall (red area).

$$\delta = \beta - \upsilon. \tag{4}$$

Subsequently, a parameter λ is defined to determine whether the contact of the drill-pipe with borehole wall has occurred or not. When $\delta \leq 0$, a drill-pipe has no contact with a borehole wall and consequently there is no contact force, hence $\lambda = 0$, otherwise, $\lambda = 1$.

$$\lambda = \begin{cases} 0, & \delta \leq 0, \\ 1, & \delta > 0. \end{cases} \tag{5}$$

Based on the simplifying assumptions, the contact is described by a linear elastic model. So, the normal force F_n can be defined as

$$F_n = \lambda \left(k_p \delta + c_p v_n \right), \tag{6}$$

where k_p and c_p represent the contact stiffness and damping between a drill-pipe and a borehole wall, respectively. v_n is the normal velocity of the drill-pipe and can be given by

$$v_n = \dot{x}_1 \cos\psi + \dot{y}_1 \sin\psi, \tag{7}$$

where ψ is the angle describing a drill-pipe whirling around the borehole axis, which can be determined from the geometries depicted in Figs. 3 and 4.

If a contact occurs, a drill-pipe motion relative to a borehole wall may be described as either pure rolling or sliding, but their co-existence has yet reported [9]. In this article, the relative velocity between the two contact surfaces v_r, which is expressed as Eq. (8), is introduced to decide whether there is sliding or not. When $v_r \neq 0$, it means that there is only relative slipping. Conversely, when $v_r = 0$, it indicates that there is no relative slipping but only pure rolling. The tangential force F_t is often approximated by Eq. (9) on the basis of regularized Coulomb friction model in [28, 29].

$$v_r = -\dot{x}_1 \sin\psi + \dot{y}_1 \cos\psi + \frac{D_{p_1}}{2}\dot{\phi}_1, \tag{8}$$

$$F_t = \mu_r \left[\tanh\left(\frac{V_r}{\chi}\right) + \frac{V_r/\chi}{1 + (V_r/\chi)^2} \right] F_n, \tag{9}$$

where μ_r is the dynamic friction coefficient. χ is the steepness parameter and it determines the range of static friction behaviour. The effect of χ on the friction coefficient between drill-pipe and borehole wall is depicted in Fig. 5. It can be seen that the increase of χ will improve the accuracy of approximation, especially for v_r close to 0. However, a large χ will make the system differential equation numerically stiff, which will increase computational cost. Therefore, χ=0.5 is employed in this article.

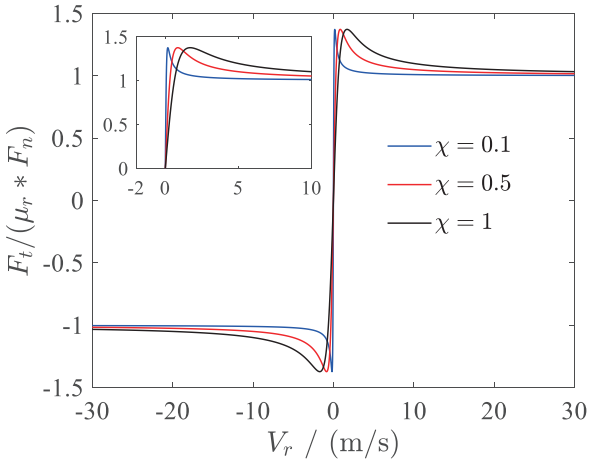

Figure 5: Relationship between the relative velocity v_r and friction coefficient under different steepness parameter χ, where the partial diagram from -2 to 10 m/s highlights the effect of χ.

Based on Fig. 4, F_{1x} and F_{1y} can be calculated by the vector superposition of the contact force components along the respective x and y directions, as expressed in Eq. (10). When the contact between the drill-pipe and borehole wall occurs, the friction torque on the drill-pipe can be written as Eq. (11).

$$\begin{aligned} F_{1x} &= -F_n \cos\psi + F_t \sin\psi, \\ F_{1y} &= -F_n \sin\psi - F_t \cos\psi. \end{aligned} \tag{10}$$

$$T_1 = \frac{1}{2} F_t D_{p_1}, \tag{11}$$

3.2. Interaction between a drill-bit and a rock

In downhole operations, a drill-bit penetrates into a rock formation with axial and angular velocities (see Fig. 6a), forming a typical bottom hole morphology shown in Fig. 6b (for more details see [30]). In order to better describe this complex behaviour mathematically, an idealized drill-bit of radius $a = D_b/2$, which consists of N identical radial blades spaced by an angle $2\pi/N$, is employed in this paper, as shown in Fig. 6c. Each blade is characterized by a sub-vertical cutting surface and a wear flat of constant length ℓ_N orthogonal to the cutting surface [31], as shown in Fig. 6d. Because the lateral motions are restricted, the instantaneous depth of cut for each blade $d_N(t)$ is identical and can be represented as

$$d_N(t) = z_2(t) - z_2\left(t - t_n(t)\right), \tag{12}$$

where a state-dependent delay $t_n(t)$ denotes the time requested for the drill-bit to rotate an angle $2\pi/N$ to its current angular position at time t. It can be obtained from the geometry that $t_n(t)$ is the solution of the following implicit equation

$$\phi_2(t) - \phi_2\left(t - t_n(t)\right) = 2\pi/N, \tag{13}$$

It can be assumed that the equivalent wear flat length of the drill-bit is $\ell = N\ell_N$ and its combined depth of cut is simply $d = Nd_N(t)$. According to the previous efforts [31–35], both W_b and T_b can be decomposed into a cutting component and a friction component as follow

$$W_b = W_{bc} + W_{bf}, \quad T_b = T_{bc} + T_{bf}. \tag{14}$$

where the subscripts bc and bf denote the cutting component and friction component, respectively. Therefore, the cutting components of WOB W_{bc} and TOB T_{bc} can be given by

$$W_{bc} = \varepsilon a \zeta d, \quad T_{bc} = \frac{1}{2}\varepsilon a^2 d. \tag{15}$$

Meanwhile, the friction components of WOB W_{bf} and TOB T_{bf} can be written as follow

$$W_{bf} = a\ell\sigma, \quad T_{bf} = \frac{1}{2}\mu_{cd}a^2\gamma\ell\sigma. \tag{16}$$

In the above equations, ε is the intrinsic specific energy of rock, which denotes the required energy to fracture a unit volume of rock. σ is the contact strength between the drill-bit and rock. ζ is a parameter characterizing the inclination of cutter face. μ_{cd} represents the dynamic friction coefficient for the interaction between the drill-bit and rock. γ is a drill-bit geometry parameter characterizing the spatial distribution of wearflat.

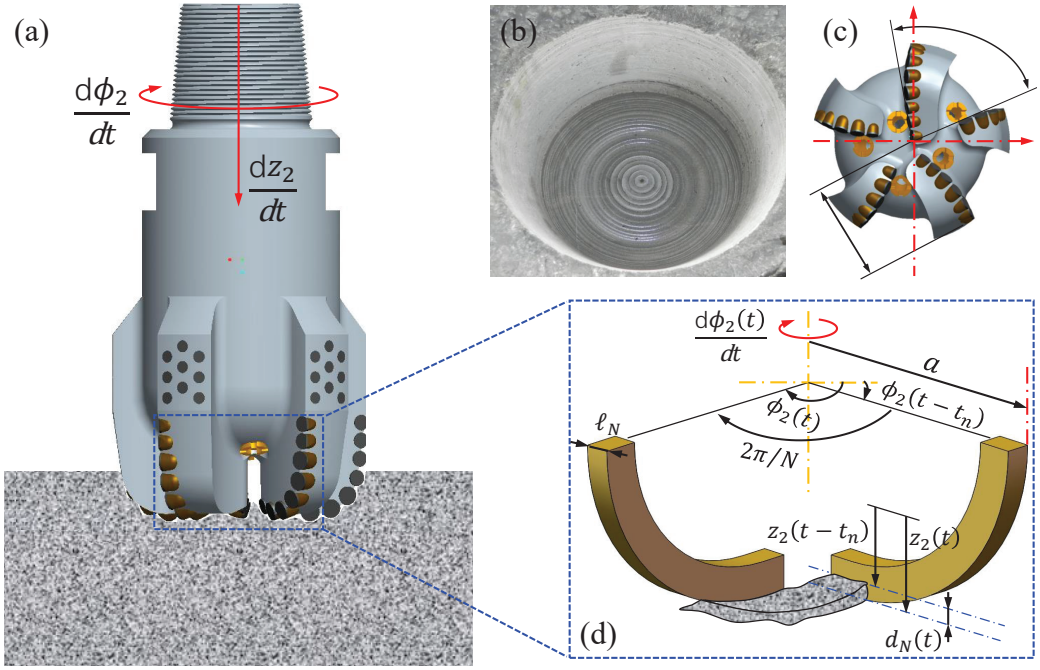

Figure 6: (a) Schematic of a drill-bit penetrating into a rock formation; (b) bottom hole morphology formed by bit-rock interaction; (c) structure and distribution parameters of drill-bit blades; (d) sketch to model regenerative effect at the borehole in bit-rock interaction using profile between two successive blades of drill-bit.

The interaction laws between a drill-bit and a rock formation are complex as they involve friction, plastic deformation, fracture, dynamics and uncertain boundary conditions. In order to facilitate the analysis, it is assumed that friction torque T_{bf} will not promote backward whirl of the drill-bit [25, 34]. So, the different interaction modes between a drill-bit and a rock can be classified into one of five modes:

- Mode 1 ($\dot{\phi}_2 > 0$, $d \geq 0$ and $\dot{z}_2 > 0$) is the *normal cutting mode*, in which a drill-bit moves forward and penetrates into a rock.

- Mode 2 ($\dot{\phi}_2 > 0$, $d \geq 0$ and $\dot{z}_2 < 0$) is considered as the *retracting cutting mode*. In this mode, a

drill-bit cuts a rock but moves backwards, which leads to the loss of contact between its wearflat and a rock.

- Mode 3 ($\dot{\phi}_2 > 0$, $d \geq 0$ and $\dot{z}_2 = 0$) is defined as the *no progression mode*, in which the axial velocity of the drill-bit is zero.

- Mode 4 ($d < 0$) is corresponding to be the *bit bouncing mode*. In this mode, a drill-bit completely separates from a rock.

- Mode 5 ($\dot{\phi}_2$=0 and $d \geq 0$) is the *stick mode*. In this mode, the angular velocity of the drill-bit is zero, and during this phase the elastic energy in a drill-string builds up leading to a so-called slip and potentially to the dangerous stick-slip phenomenon. The slip can manifest itself in either Mode 1, 2 or 3.

In this paper, all parameters are chosen for a typical deviated, and even a horizontal borehole configuration as reported in [22]. The rock cutting model parameters can vary in a large extend but are chosen as shown in Table 3 for the sake of comparison with the existing literature [25].

Table 3: Parameters used to determine contact mechanics models.

Parameter	Value	Unit	Parameter	Value	Unit
k_p	1×10^8	N/m	ℓ	3.8×10^{-3}	m
c_p	5×10^3	Ns/m	γ	1	/
χ	0.5	/	ζ	0.6	/
μ_r	0.01-0.6	/	ε	60	MPa
μ_{cd}	0.6	/	σ	60	MPa

4. Model verification under various conditions

In order to investigate the robustness of the overall dynamic model established in Sections 2 and 3, the friction and cutting effects are gradually switched on and even *Disk 1* and *Disk 2* are treated as one, as explained below. In this section, we pay more attention to open or closed of the contact scenarios, so that both the constant gravity $m_1 g$ and buoyancy force F_u are neglected, just like the dynamic model of drill-string in a vertical well. The Euler-forward finite difference numerical integration technique (see Appendix B), is used to compute dynamic responses.

Case I: No drilling with *Disk 1* and *Disk 2* as an integral part. The axial and lateral motions of the drill-string are switched off, so that it can be considered as a torsion pendulum with 1 DOF. Under

this circumstance, rock cutting is not accounted for, so just the friction effect is considered. For this case, the dynamic model can be written as

$$J\ddot{\phi} + \tilde{c}_t\dot{\phi} + \tilde{k}_t\left(\phi - \phi_t\right) = -T_b, \tag{17}$$

where J is the total moment of inertia of the drill-string. T_b is the friction torque. $\tilde{k}_t$ is the torsional stiffness of the drill-string for Case I and is expressed by Eq. (18) by referring to the method explained in Appendix A. $\tilde{c}_t$ is the torsional damping calculated from damping ratio $\tilde{\xi}$.

$$\tilde{k}_t = \frac{GI_0}{L_p}, \quad \tilde{\xi} = \frac{\tilde{c}_t}{2\sqrt{\tilde{k}_t J}}. \tag{18}$$

Specifically, T_b is determined by a combination of the switch model and the dry friction model [24], as expressed by Eq. (19), which makes the dynamic model discontinuous and causes complex dynamical phenomena, such as stick-slip.

$$T_b = \begin{cases} T_{eb} = \tilde{k}_t\left(\phi_t - \phi\right) - \tilde{c}_t\dot{\phi}, & \left|\dot{\phi}\right| < D_v \text{ and } \left|T_{eb}\right| \le \left|T_{sb}\right|, \\ T_{sb}\mathrm{sgn}\left(T_{eb}\right) = \mu_{sd} a W_0 \mathrm{sgn}\left(T_{eb}\right), & \left|\dot{\phi}\right| < D_v \text{ and } \left|T_{eb}\right| > \left|T_{sb}\right|, \\ aF_0\left[\mu_{cd} + \left(\mu_{sd} - \mu_{cd}\right)\exp\left(-\gamma_b / v_f\left|\dot{\phi}\right|\right)\right]\mathrm{sgn}\left(\dot{\phi}\right), & \left|\dot{\phi}\right| \ge D_v, \end{cases} \tag{19}$$

where T_{eb} is the reaction torque arising from the twist of the drill-pipe, μ_{sd} is the static friction coefficient, D_v is a constant used to determine whether the drill-bit is in the stick phase, γ_b is a constant defining the decay rate of T_b whit velocity, v_f is introduced to keep the units unified.

In Fig. 7 we present example dynamic responses of the drill-string for two different values of static friction coefficient μ_{sd}. A sinusoidal driving rotation speed $\dot{\phi}_t = \vartheta_0 + A_0\sin\left(w_0 t\right)$ is used to avoid getting free oscillation responses due to the effect of torsional damping. It can be seen that adopting different values of static friction coefficient μ_{sd} will arise different dynamic responses of the drill-string. When $\mu_{sd} = 0.61$ is employed, the drill-string experiences a stable vibration without stick-slip behaviour (see Fig. 7a), however its torsional motion reveals typical features of stick-slip when the value of μ_{sd} is set equal to 0.7, as shown in Fig. 7b.

Case II: No drilling with *Disk 1* and *Disk 2* as two parts. In this case, the axial motions of both *Disk 1* and *Disk 2* are switched off on the basis of the overall model described by Eq. (2). Therefore, just the friction behaviour is considered and a sinusoidal driving rotation speed $\dot{\phi}_t = \vartheta_0 + A_0\sin\left(w_0 t\right)$ is also employed, which are similar with the pertinent setups in Case I. Likewise, the external force load W_0 is acted on *Disk 2* directly, and the friction torque arising from the interaction between the drill-bit

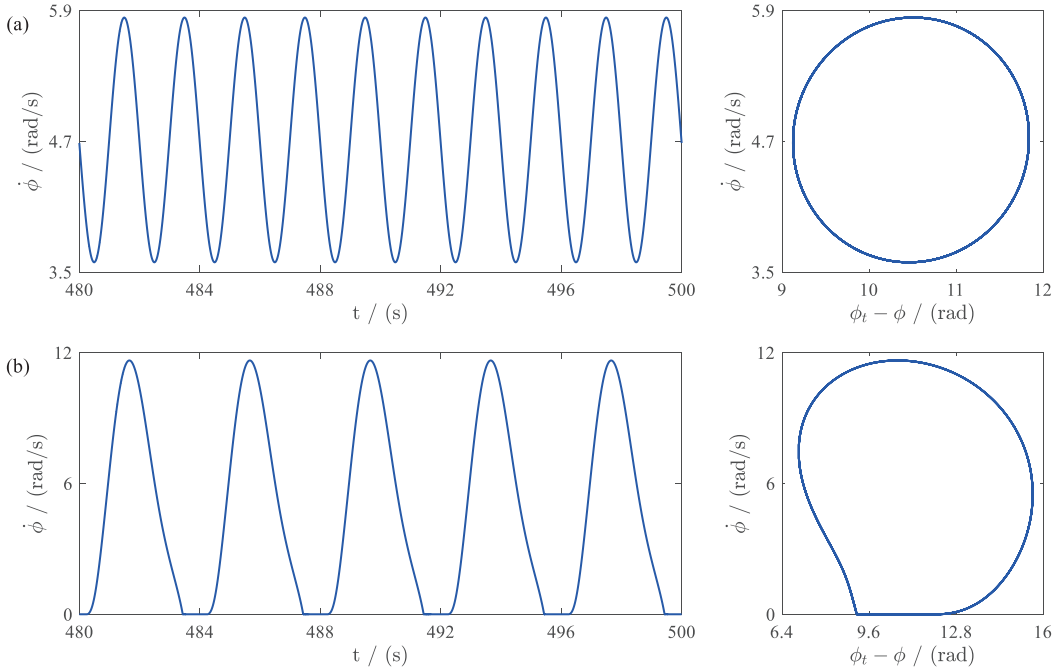

Figure 7: Time-history responses of drill-string obtained from Case I, for the parameter values $\tilde{k}_t = 469$ Nm/rad, $J = 180.5$ kgm^2, $W_0 = 75$ kN, D_v=1 $\times$ 10^{-6}, γ_b=0.9, v_f=1, $\dot{\phi}_t = 1.5\pi + \pi \sin(\pi t)$ rad/s and $\tilde{\xi} = 0.02$. (a) $\mu_{sd} = 0.61$; (b) $\mu_{sd} = 0.7$.

and rock is modeled by using Eq. (19).

The first step is restricting the lateral motions of *Disk 1*, so that the dynamic model is translated into an universal model for reproducing the torsional vibration of the drill-string. The remaining parameters keep same with these adopted in the overall model. By referencing the results obtained from Case I, we employ different values of static friction coefficient μ_{sd}, as shown in Fig. 8. It can be seen that the static friction coefficient μ_{sd} has clear implications for the dynamic responses of the drill-string. For example, both the drill-pipe and drill-bit experience periodic torsional vibration with no stick-slip when $\mu_{sd} = 0.61$ is employed, as shown in Fig. 8a. Meanwhile, the torsional vibration of the drill-bit is more intense than that of the drill-pipe under the same conditions, which is consistent with previous studies [36]. When the static friction coefficient is increased to $\mu_{sd} = 0.82$, the torsional vibration of the drill-string is also periodic but the rotation of the drill-bit has typical features of stick-slip, as shown in Fig. 8b. More interestingly, when the value of μ_{sd} is equal to 0.7, the phase spaces of both the drill-pipe and the drill-bit have strange attractors, so that their motions are chaotic, as shown in Fig. 8c.

Subsequently, the lateral motions and whirling of *Disk 1* are considered comprehensively on basis of the model in the first step. It should be noted that the model would be modified as that in the first step if the offset of the drill-pipe e is equal to 0, so that this situation will not be discussed further in current

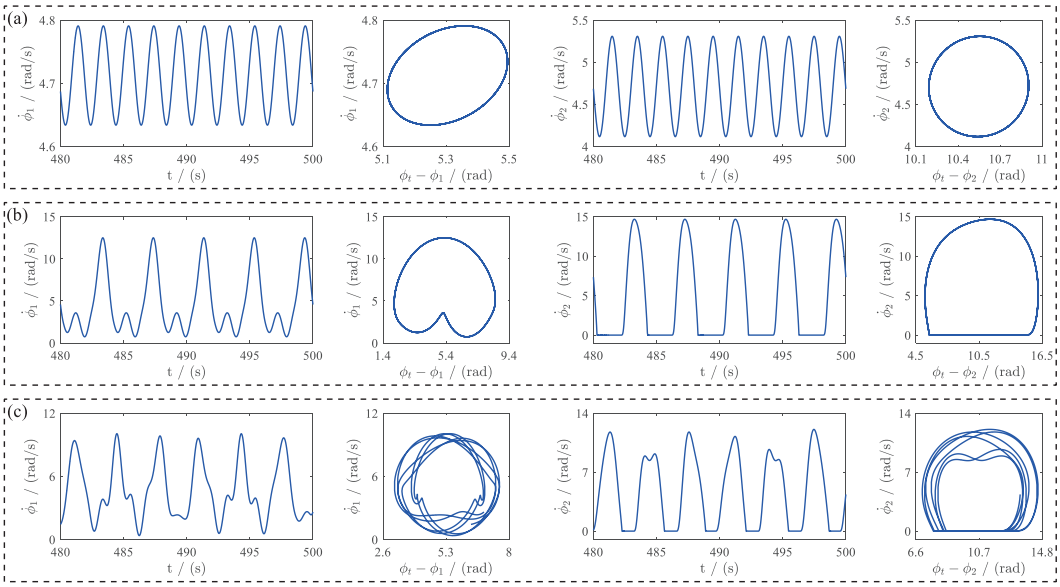

Figure 8: Drill-string responses obtained from Case II without considering the lateral motions of the drill-pipe, for the parameter values $W_0 = 75$ kN, D_v=1 $\times$ 10^{-6}, γ_b=0.9, v_f=1, $\dot{\phi}_t = 1.5\pi+\pi\sin(\pi t)/6$ rad/s and $\xi = 0.02$. (a) $\mu_{sd} = 0.61$; (b) $\mu_{sd} = 0.82$; (c) $\mu_{sd} = 0.7$.

work. The drill-string responses under different values of the dynamic friction coefficient μ_r between the drill-pipe and borehole wall are depicted in Fig. 9, which indicates that the magnitude of μ_r plays a crucial role in determining the drill-string responses.

When the dynamic friction coefficient μ_r is 0.01, as can be seen in Fig. 9a, the torsional motions of both the drill-pipe and drill-bit are periodic, and meanwhile the latter experiences a typical stick-slip. In addition, it can be observed that the drill-pipe might loss contact with the borehole wall and the random collisions occur. When the dynamic friction coefficient μ_r is increased to 0.3, the drill-pipe has both the mitigated random collisions with the borehole wall and the backward whirling, as shown in Fig. 9b. Due to the opposite sign between the slopes of ϕ_1 and ψ, the whirling direction of the drill-pipe is different with its rotation direction [15], which is depicted in panel (b) for backward whirling. Under this circumstance, the torsional motions of both the drill-pipe and the drill-bit are chaotic. With an increase in the dynamic friction coefficient μ_r to 0.6, the drill-pipe always stays in contact with the borehole wall and the random collisions between these two parts almost completely disappear. At this moment, the drill-pipe has a stable backward whirling (see Fig. 9c). The interesting thing, however, is that both the drill-pipe and the drill-bit rotate periodically again.

Case III: Drilling with *Disk 1* and *Disk 2* as an integral part. Compared with the previous two cases, the most immediate improvement is that the coupled axial-torsional vibration of the drill-string system is simulated by considering the regenerative cutting effect of the drill-bit, which are similar to

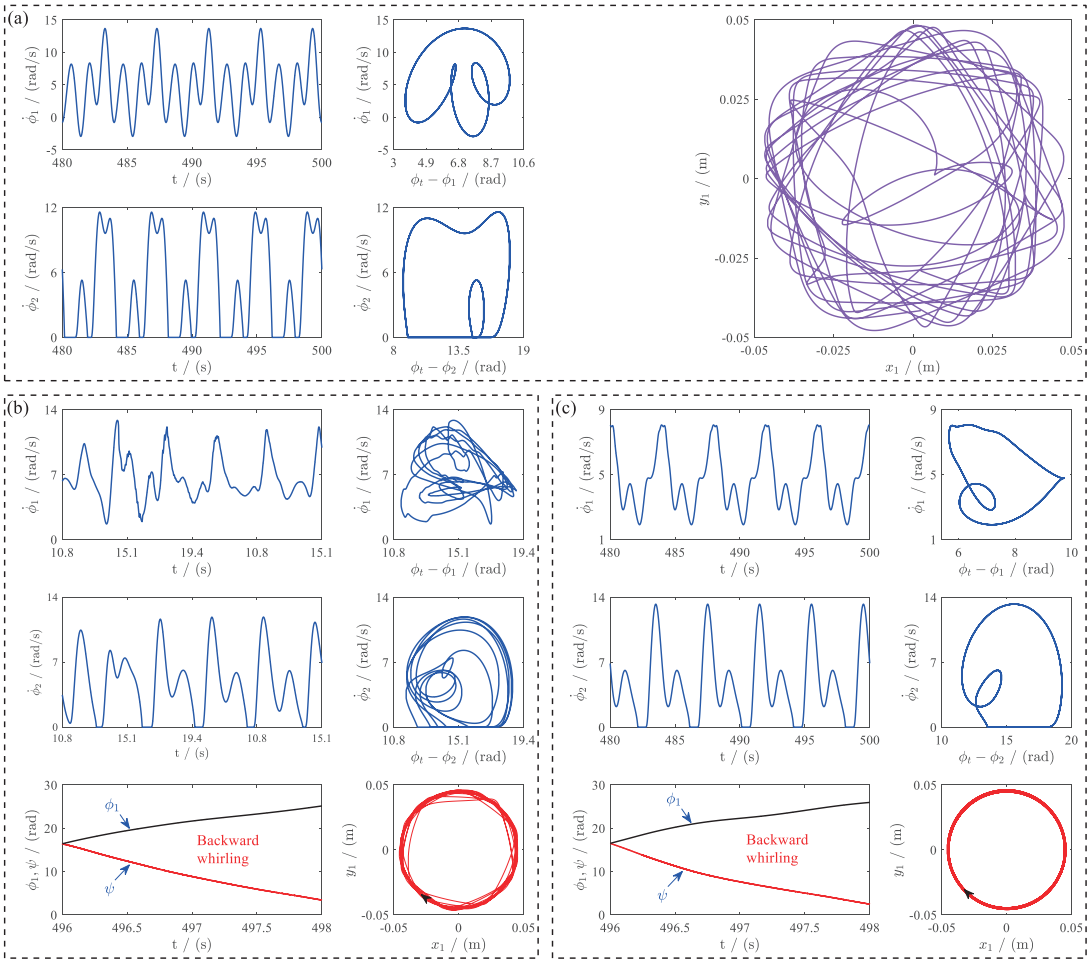

Figure 9: Drill-string responses obtained from Case II with considering the lateral motions of the drill-pipe, for the parameter values $W_0 = 100$ kN, D_v=1×10^{-6}, $\mu_{sd} = 0.75$, γ_b=0.9, v_f=1, $\dot{\phi}_t = 1.5\pi+\pi \sin(\pi t)$ rad/s, $\kappa = 0.02$ and $\xi = 0.02$, where purple and red colours represent chaotic motions and backward whirling of the drill-pipe on its cross section, respectively. (a) $\mu_r = 0.01$; (b) $\mu_r = 0.3$; (c) $\mu_r = 0.6$.

metal machining [37–39]. Due to the complexity and high nonlinearity arising from the varying time delay, even a constant driving rotation speed $\dot{\phi}_t$ would excite excessive vibration, so that a constant $\dot{\phi}_t$ is employed in this case. The top end of the drill-string is assumed to move down at a constant velocity V_0, which can be regarded as the steady-state drilling rate. However, the lateral motions of the drill-string system are switched off. Based on these, the dynamic model in this case is similar with that established in [26], which can be written as follow

$$\begin{aligned} J\ddot{\phi} + \tilde{c}_t\dot{\phi} + \tilde{k}_t\left(\phi - \phi_t\right) &= -T_b, \\ m\ddot{z} + \tilde{c}_a\dot{z} + \tilde{k}_a\left(z - V_0 t\right) &= W_0 - W_b. \end{aligned} \tag{20}$$

where $J = J_1 + J_2$ and $m = m_1 + m_2$ are the respective total moment of inertia and mass of the drill-

string. T_b and W_b are determined by the bit-rock interaction model (see Section 3.2). $\tilde{k}_t$ and $\tilde{k}_a$ represent the torsional and axial stiffness of the drill-string for Case II respectively, and are expressed as Eq. (21) by the method provided in Appendix A. $\tilde{c}_t$ and $\tilde{c}_a$ are the respective torsional and axial damping, which can be calculated from the damping ratios listed in Eq. (22).

$$\tilde{k}_t = \frac{GI_0}{L_p}, \quad \tilde{k}_a = \frac{EA}{L_p}. \tag{21}$$

$$\tilde{\xi} = \frac{\tilde{c}_t}{2\sqrt{\tilde{k}_t J}}, \quad \tilde{\eta} = \frac{\tilde{c}_a}{2\sqrt{\tilde{k}_a m}}. \tag{22}$$

The torsional and axial responses of drill-string under different driving rotation speeds are shown in Fig. 10. When the driving rotation speed $\dot{\phi}_t$ is 5.92 rad/s, both the rotational and axial motions of the drill-string are periodic and the former shows typical stick-slip characteristics, as shown in Fig. 10a. With the increase of the driving rotation speed $\dot{\phi}_t$, the stick-slip effect of the drill-string gradually weakens and finally disappear completely. When the driving rotation speed $\dot{\phi}_t$ is increased to 9.9 rad/s, the rotation and axial motions of the drill-string are also periodic but have no stick-slip phenomenon, as shown in Fig. 10b. However, the drill-string responses may be chaotic, for example, these under $\dot{\phi}_t$=7.85 rad/s, as shown in Fig. 10c. Interestingly, the average rates of penetration obtained from both this three scenarios are equal to the value of V_0 (5.9 mm/s).

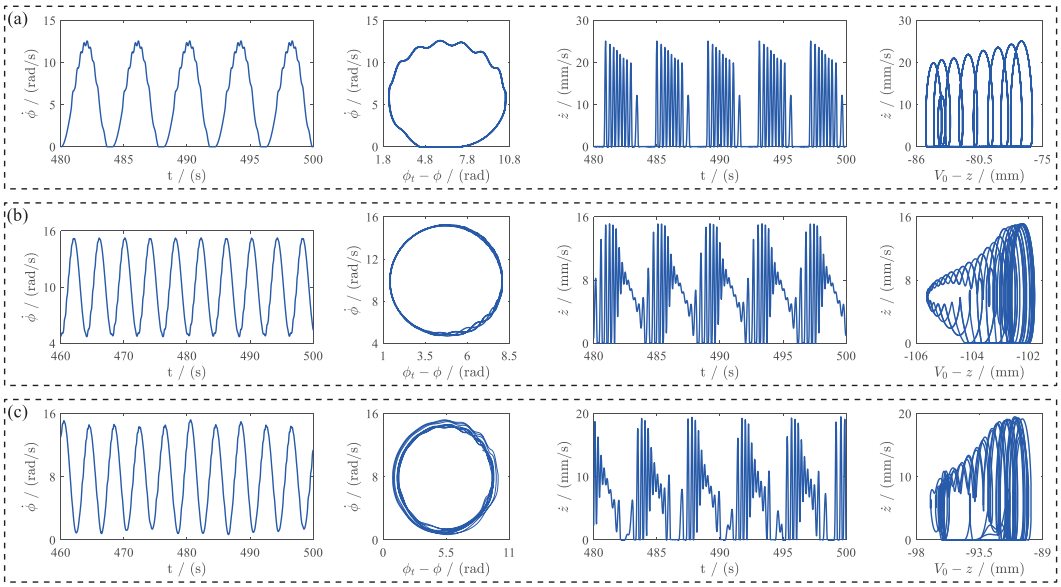

Figure 10: Drill-string responses obtained from Case III, for the parameter values $\tilde{k}_t$ = 469 Nm/rad, $\tilde{k}_a = 3.5 \times 10^5$ N/m, $\tilde{\xi} = 0.02$, $\tilde{\eta} = 0.02$, $m = 5.3 \times 10^4$ kg, $J = 180.5$ kgm^2, $W_0 = 75$ kN and $V_0 = 5.9$ mm/s. (a) $\dot{\phi}_t$=5.92 rad/s; (b) $\dot{\phi}_t$=9.9 rad/s; (c) $\dot{\phi}_t$=7.85 rad/s.

Case IV: Drilling described by the overall model. In this case, the axial, torsional and lateral motions of the drill-string are coupled to each other, with considering both the regenerative cutting effect of the drill-bit and the intermittent contact of the drill-pipe with the borehole wall. Meanwhile, the whirling of the drill-pipe can also be observed. The values of corresponding parameters are listed in Tables 1, 2 and 3. In the overall model, the effects of both the axial, torsional and lateral damping are considered (η=0.02, κ=0.02 and ξ=0.02).

In the first step, we still just consider the axial and torsional motions of the drill-string, so that the eccentricity of the drill-pipe e is taken as 0 under this circumstance. Fig. 11a shows the obtained axial and torsional responses of the drill-string. It can be seen that even a constant excitation can also cause violent vibrations of the drill-string due to the regenerative cutting effect. Meanwhile, both the axial and torsional vibration of the drill-bit are more intense than these of the drill-pipe, which is consistent with the conclusions obtained from Case II (see Fig. 8).

Then, the lateral motions and whirling of the drill-pipe are introduced into the model in the first step. When the driving rotation speed $\dot{\phi}_t$ is decreased to 3π rad/s, the torsional vibration and axial vibration of both the drill-pipe and drill-bit become more intense than these obtained from the model in the first step, as shown in Figs. 11b and 11c. Meanwhile, the motions of the drill-bit have obvious stick-slip features, and the stick phase will become more durable as the dynamic friction coefficient μ_r increasing. In addition, when the dynamic friction coefficient μ_r is set to 0.01, the random collisions between the drill-pipe and borehole wall occur, and the loss of contact is significant, as can be seen in Fig. 11b. When the dynamic friction coefficient μ_r is increased to 0.6, the drill-pipe always keeps contact with the borehole wall and a stable backward whirling occurs, as shown in Fig. 11c. This trend is consistent with that obtained from Case II.

In summary, the results obtained from the above four cases are always stable. By comprehensively examining the physical behaviors for all these four cases, we can say that the proposed dynamic model is robust, so that it can be used to further investigations into the nonlinear dynamic behaviors of a drill-string in a horizontal well.

5. Whirling of a horizontal drill-string

In this section, we will further investigate the complicated whirling of a horizontal drill-string during drilling operations by using the overall model, which is expressed as Eq. (2). It should be noted that the constant gravity $m_1 g$ and buoyancy force F_u of the drill-pipe are applied on *Disk 1* in y direction, which is different with the models in Section 4.

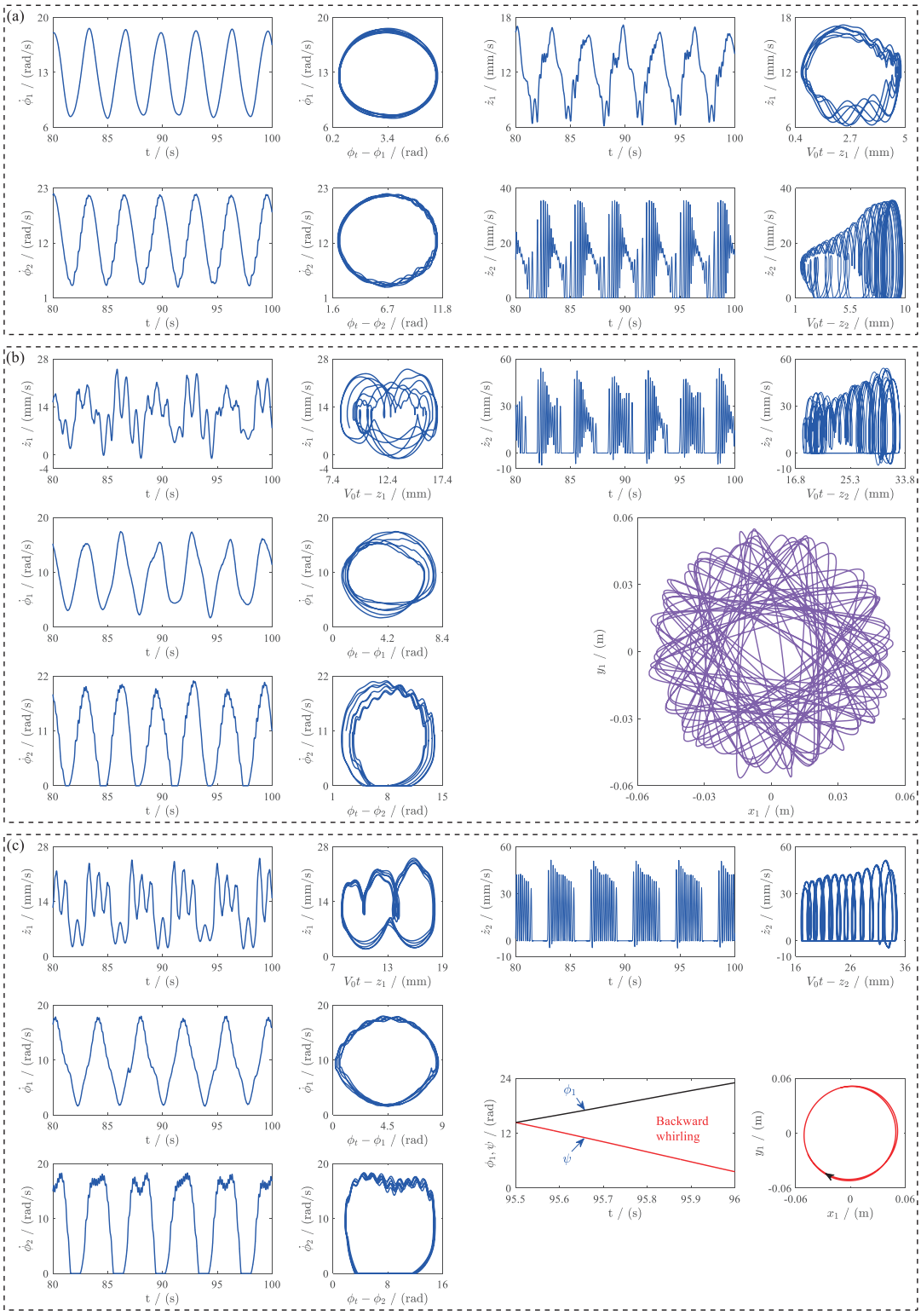

Figure 11: Drill-string responses obtained from Case IV under different conditions, for the parameter values $W_0 = 45$ kN and $V_0 = 12$ mm/s, where purple and red colours represent chaotic motions and backward whirling of the drill-pipe on its cross section, respectively. (a) $\dot{\phi}_t = 4\pi$ rad/s and $e = 0$; (b)$\dot{\phi}_t = 3\pi$ rad/s, $e = 0.008$ and $\mu_r = 0.01$; (c) $\dot{\phi}_t = 3\pi$ rad/s, $e = 0.008$ and $\mu_r = 0.6$.

5.1. Influence of driving rotation speed

The obtained trajectories of drill-pipe center for different driving rotation speeds are illustrated in Fig. 12. When the driving rotation speed $\dot{\phi}_t$ is set to $5\pi/3$ rad/s, the drill-pipe is always at the bottom left (the third quadrant) of the borehole and its range of motion never exceeds the borehole center, as shown in Fig. 12a. On this occasion, the drill-pipe has a small-scale revolution around the borehole axis but whirling does not occur. With the increase of the driving rotation speed $\dot{\phi}_t$, the climbing distance of the drill-pipe along the borehole wall increases. When the driving rotation speed $\dot{\phi}_t$ is increased to $8\pi/3$ rad/s, the contact area between the drill-pipe and borehole wall has a significant increase, and the drill-pipe can reach the second and forth quadrant of the borehole, as shown in Fig. 12b. We say that the drill-pipe experiences a local whirling. When the driving rotation speed $\dot{\phi}_t$ is 4π rad/s, the motion locus of the drill-pipe almost fills up the whole borehole. In this situation, global whirling and contact occur, accompanied by random collisions, as shown in Fig. 12c. With an increase in the driving rotation speed $\dot{\phi}_t$ to 5π rad/s, the drill-pipe always keeps contact with the borehole wall and experiences a stable whirling, as seen in Fig. 12d.

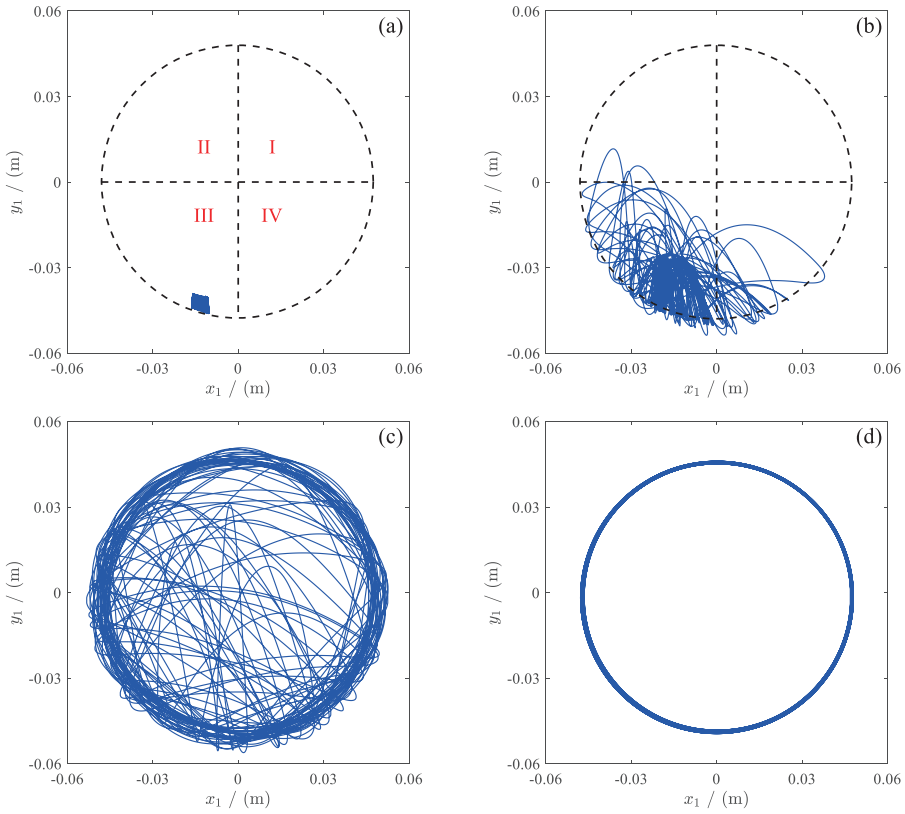

Figure 12: Trajectories of drill-pipe center for the parameter values $\mu_r = 0.3$, $W_0 = 45$ kN and $V_0 = 6$ mm/s under different driving rotation speeds. (a) $\dot{\phi}_t = 5\pi/3$ rad/s; (b) $\dot{\phi}_t = 8\pi/3$ rad/s; (c) $\dot{\phi}_t = 4\pi$ rad/s; (d) $\dot{\phi}_t = 5\pi$ rad/s.

Fig. 13 shows the whirling speeds of drill-pipe under different driving rotation speeds. As can be seen from Figs. 13a and 13b, when the driving rotation speed $\dot{\phi}_t$ is from $5\pi/3$ to $8\pi/3$ rad/s, the drill-pipe experiences forward whirling together with backward whirling, and its forward whirling speed is approximately equal to backward whirling speed. When the driving rotation speed $\dot{\phi}_t$ is increased to 4π rad/s, the drill-pipe experiences backward whirling for the majority of time, and its instantaneous forward whirling is caused by random collision with the borehole wall, as shown in Fig. 13c. When the driving rotation speed $\dot{\phi}_t$ raises to 5π rad/s, the stable whirling of the drill-pipe is always backward (see Fig. 13d), and the maximum whirling speed even can reach to 1.5 times of the driving rotation speed $\dot{\phi}_t$, which indicates that a very intense backward whirling will occur under a high driving rotation speed. As a result, the risk of drill tools damage will be greatly improved.

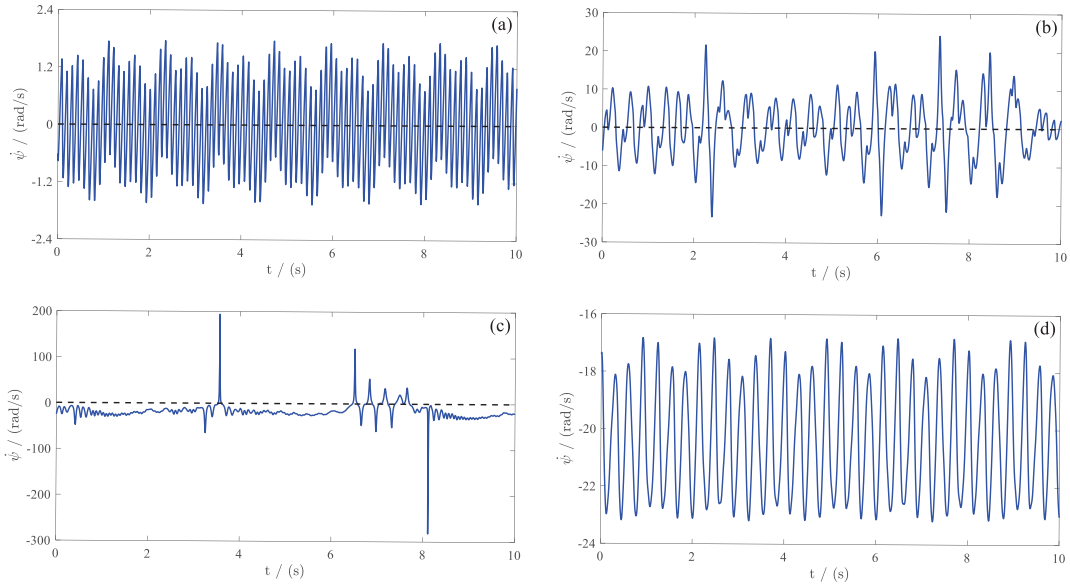

Figure 13: Whirling speeds of drill-pipe for the parameter values $\mu_r = 0.3$, $W_0 = 45$ kN and $V_0 = 6$ mm/s under different driving rotation speeds, where the black dotted lines represent $\dot{\psi} = 0$ rad/s. (a) $\dot{\phi}_t = 5\pi/3$ rad/s; (b) $\dot{\phi}_t = 8\pi/3$ rad/s; (c) $\dot{\phi}_t = 4\pi$ rad/s; (d) $\dot{\phi}_t = 5\pi$ rad/s.

5.2. Influence of dynamic friction coefficient

The dynamic friction coefficient μ_r is another parameter that can influence the trajectory of drill-pipe center. Fig. 14 depicts the dependence of trajectory of drill-pipe center on the dynamic friction coefficient μ_r. When the dynamic friction coefficient μ_r is 0.01, the drill-pipe collides with the borehole wall randomly and its trajectory apparently fails to reach the top of borehole due to the effect of gravity, as shown in Fig. 14a. However, the friction force arising from the borehole wall is too small to support the climb of the drill pipe in this situation, so that whirling doesn't occur. When the dynamic friction coefficient

μ_r is 0.15, the random collisions between the drill-pipe and borehole wall are essentially erased and the friction force drives the drill-pipe to climb along the borehole wall, as shown in Fig. 14b. Likewise, the small-scale revolution of the drill-pipe at this point is also too far from whirling. With the increase of the dynamic friction coefficient μ_r, the drill-pipe can gradually climb to higher altitudes, as shown in Figs. 14c and 14d. For example, the drill-pipe has a local whirling when the dynamic friction coefficient μ_r is set to 0.3 (see Fig. 14c), and a global whirling appears with the dynamic friction coefficient μ_r increased to 0.6 (see Fig. 14d), even though random collisions still happen from time to time.

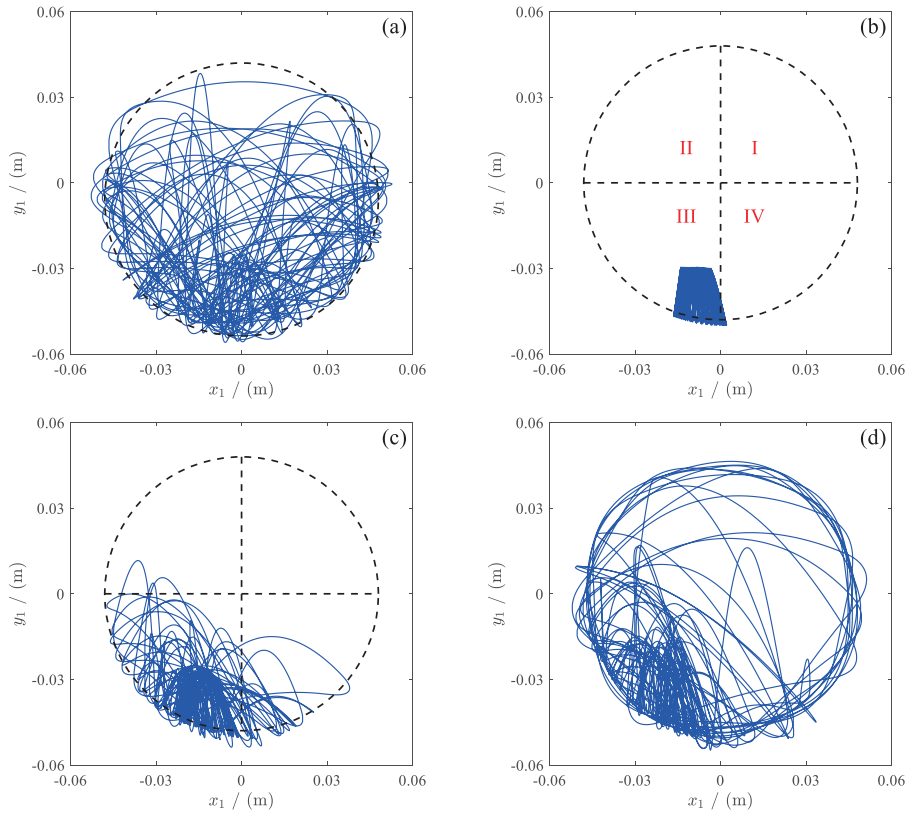

Figure 14: Trajectories of drill-pipe center for the parameter values $\dot{\phi}_t = 8\pi/3$ rad/s, $W_0 = 45$ kN and $V_0 = 6$ mm/s under different dynamic friction coefficients. (a) $\mu_r = 0.01$; (b) $\mu_r = 0.15$; (c) $\mu_r = 0.3$; (d) $\mu_r = 0.6$.

Moreover, referring to the previous analysis results of Figs. 12a, 12b, 13a and 13b, it can be concluded that the forward and backward whirling of the drill-pipe coexist and appear alternately when the dynamic friction coefficient μ_r is set from 0.15 to 0.3. However, Fig. 15 indicates that the global whirling of the drill-pipe is essentially backward when the dynamic friction coefficient μ_r is increased to 0.6, which is similar with the results obtained from increasing the driving rotation speed $\dot{\phi}_t$ (see Fig. 13c). Likewise, the mutations of the whirling speed shown in Fig. 15 are also caused by the random collisions between

the drill-pipe and borehole wall.

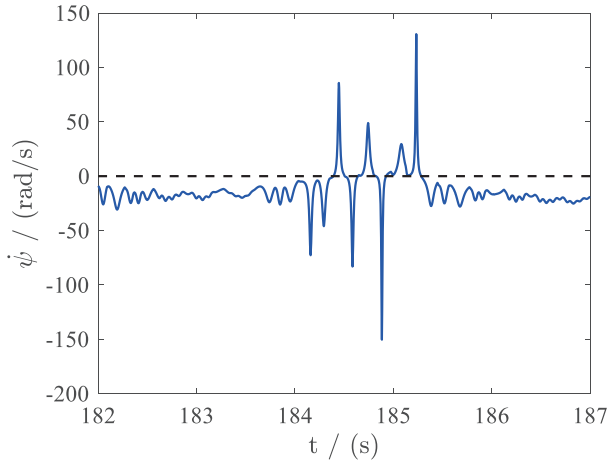

Figure 15: Whirling speed of drill-pipe for the parameter values $\mu_r = 0.6$, $\dot{\phi}_t = 8\pi/3$ rad/s, $W_0 = 45$ kN and $V_0 = 6$ mm/s, where the black dotted line represents $\dot{\psi} = 0$ rad/s.

6. Concluding remarks

In this paper we have developed a 6-DOF dynamic model to investigate the axial, lateral and torsional vibration of a drill-string in a horizontal well. This model involves the interactions of a drill-pipe with a borehole wall and a drill-bit with a rock formation. A particular attention is devoted to the different motion regimes and regenerative cutting effect of the drill-bit, which will introduce a state dependent time delay into the governing equations, so that the motions in different directions are successfully coupled.

Subsequently, the established dynamic model is systematically checked where the friction and cutting effects are gradually switched on, which highlights the critical roles of the regenerative cutting effect of the drill-bit and friction behaviors between the drill-pipe and borehole wall in our model. Meanwhile, the robustness of the dynamic model is verified. Therefore, we can use this model to further explore the nonlinear dynamic characteristics of drill-string in horizontal wells, which will lay a theoretical foundation for optimizing drilling parameters.

Finally, the validated dynamic model is used to study the whirling of a horizontal drill-pipe, and a particular attention is given to the influence of driving rotation speed and dynamic friction coefficient on whirling. The research results show that increasing driving rotation speed and dynamic friction coefficient will increase the contact area between the drill-pipe and borehole wall, so that the climb distance of the drill-pipe and its range of motion enlarge. In addition, when the driving rotation speed and dynamic friction coefficient are at a low level, whirling does not occur. When these two parameters are increased to

a special range, the drill-pipe experiences a local whirling, which is marked by the coexistence of forward whirling and backward whirling. When the driving rotation speed and dynamic friction coefficient increase to a threshold, a global whirling appears and its direction is mainly backward. If the driving rotation speed keeps increasing, a drill-pipe can even experience a steady backward whirling.

Acknowledgments

The authors cordially acknowledge the financial support from the Science and Technology Planning Project of Sichuan Province (Grant No.: 18YYJC1146) and the Science and Technology Innovation Seedling Project of Sichuan Province (Grant No.: 2018092).

Furthermore, special thanks of the first author to his girlfriend Yuan Yuan for her support and understanding. Her encouragement and companionship supported the first author to finish so many iterations of this paper in a foreign land.

Appendix A. Derivation of Equations of Motion

As Fig. 2 illustrates, the kinetic energy of the horizontal drill-string system includes two parts, one is the drill-pipe (*Disk 1*), the other is the BHA (*Disk 2*). *Disk 1* has a mass m_1 and a moment of inertia J_1. *Disk 2* has a mass m_2 and a moment of inertia J_2. Hence, the kinetic energy of the drill-string system can be written as

$$T = \frac{1}{2}m_1\left(\dot{x}_1^2 + \dot{y}_1^2 + \dot{z}_1^2\right) + \frac{1}{2}J_1\dot{\phi}_1^2 + \frac{1}{2}m_2\dot{z}_2^2 + \frac{1}{2}J_2\dot{\phi}_2^2, \tag{23}$$

where a dot over a parameter indicates its derivative with respect to time t. The potential energy V of the drill-string system consists of two main elements: the gravitational potential energy V_g and the elastic potential energy V_e, as shown below.

$$V = V_g + V_e = m_1 g y_1 + V_e. \tag{24}$$

In order to express V_e, the pipeline which is formed by screwing drill-pipes to each other, is modeled by using a Euler-Bernoulli beam due to its small ratio diameter/length, approximately equal to 10^{-4}. Let $w(z,t)$ and $\theta(z,t)$ be the respective axial and torsional displacements of the pipeline, $u(z,t)$ and $v(z,t)$ be its lateral displacements at $z \in [0, L_p]$ and at time t. We assume that pipeline deformation is linearly elastic, so V_e can be constructed as

$$V_e = \frac{EA}{2}\int_0^{L_p}(w')^2\mathrm{d}z + \frac{GI_0}{2}\int_0^{L_p}(\theta')^2\mathrm{d}z + \frac{EI_x}{2}\int_0^{L_p}\left((u'')^2+(v'')^2\right)\mathrm{d}z. \tag{25}$$

where a single prime and a double prime denote the first and second partial derivatives with respect to z, respectively. A, I_0 and I_x are the respective sectional area, polar moment of inertia and inertia moment of the drill-pipe cross section, and can be determined as

$$\begin{aligned} A &= \tfrac{\pi}{4}\left(D_{p1}^2 - D_{p2}^2\right), \\ I_0 &= \tfrac{\pi}{32}\left(D_{p1}^4 - D_{p2}^4\right), \\ I_x &= \tfrac{\pi}{64}\left(D_{p1}^4 - D_{p2}^4\right). \end{aligned} \tag{26}$$

According to the simplified model depicted in Fig. 2, the pipeline is divided into two sections based on the Finite Element Method (FEM). Therefore, the boundary conditions associated with axial motion of the pipeline are of the form

$$\begin{cases} w|_{z=0} = V_0 t, \\ w|_{z=\frac{L_p^-}{2}} = w|_{z=\frac{L_p^+}{2}} = z_1, \\ w|_{z=L_p} = z_2. \end{cases} \tag{27}$$

Meanwhile, we assume that the axial displacement $w(z,t)$ of the pipeline versus z appears to be linear at both $z \in [0, L_p/2]$ and $z \in [L_p/2, L_p]$. Therefore, $w(z,t)$ can be expressed as follow

$$w(z,t) = \begin{cases} \frac{z_1 - V_0 t}{L_p/2} z + V_0 t, & 0 \le z \le \frac{L_p}{2}, \\ \frac{z_2 - z_1}{L_p/2} z + 2z_1 - z_2, & \frac{L_p}{2} < z \le L_p. \end{cases} \tag{28}$$

In addition, the boundary conditions associated with axial motion of the pipeline can be given by

$$\begin{cases} \theta|_{z=0} = \phi_t, \\ \theta|_{z=\frac{L_p^-}{2}} = \theta|_{z=\frac{L_p^+}{2}} = \phi_1, \\ \theta|_{z=L_p} = \phi_2. \end{cases} \tag{29}$$

Similarly, the angular displacement $\theta(z,t)$ also varies with z linearly at both $z \in [0, L_p/2]$ and $z \in [L_p/2, L_p]$. So, $\theta(z,t)$ can be written as follow

$$\theta(z,t) = \begin{cases} \frac{\phi_1 - \phi_t}{L_p/2} z + \phi_t, & 0 \le z \le \frac{L_p}{2}, \\ \frac{\phi_2 - \phi_1}{L_p/2} z + 2\phi_1 - \phi_2, & \frac{L_p}{2} < z \le L_p. \end{cases} \tag{30}$$

Furthermore, the bending deflection of the pipeline in x direction can be depicted in Fig. 16, in which the pipeline experiences a symmetric bending caused by a concentrated load at $z = L_p/2$. As can be seen in Fig. 16, the boundary conditions associated with bending deflection in x direction can be given by

$$\begin{cases} u|_{z=0} = u|_{z=L_p} = 0, \\ \theta|_{z=\frac{L_p}{2}} = x_1. \end{cases} \tag{31}$$

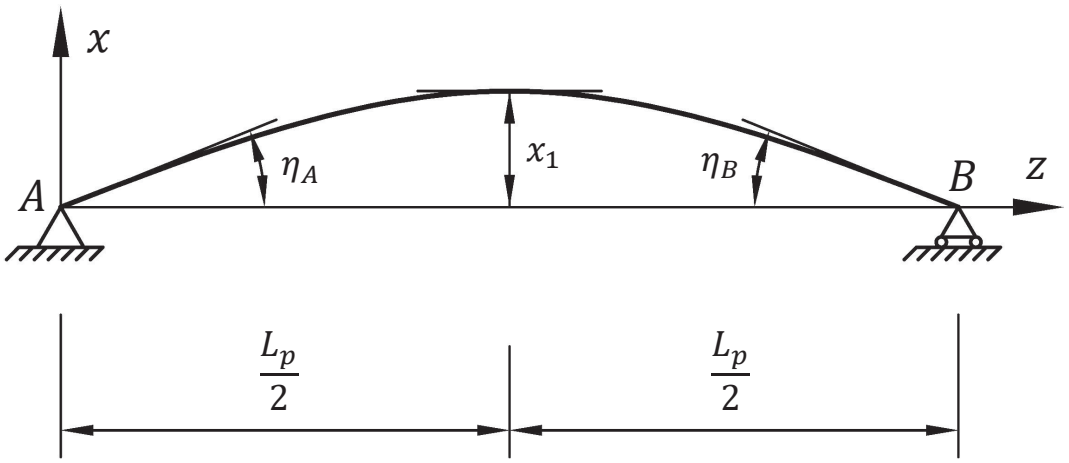

Figure 16: Schematic of bending deflection of the pipeline in x direction.

On this basis, the deflection equation of the pipeline in x direction can be determined as Eq. (32). At this moment, the angles of rotation of its left and right transverses can be given by $\eta_A = \eta_B = 3x_1/L_p$, which are always ignored due to small order of magnitude. Bending in y direction is symmetric to that in x direction, so that $v\,(z,t)$ can be obtained as Eq. (33).

$$u(z,t) = \begin{cases} \frac{x_1}{L_p^3}\left(3L_p^2 z - 4z^3\right), & 0 \le z \le \frac{L_p}{2}, \\ \frac{x_1}{L_p^3}\left(3L_p^2\left(L_p - z\right) - 4(L_p - z)^3\right), & \frac{L_p}{2} < z \le L_p. \end{cases} \tag{32}$$

$$v(z,t) = \begin{cases} \frac{y_1}{L_p^3}\left(3L_p^2 z - 4z^3\right), & 0 \le z \le \frac{L_p}{2}, \\ \frac{y_1}{L_p^3}\left(3L_p^2\left(L_p - z\right) - 4(L_p - z)^3\right), & \frac{L_p}{2} < z \le L_p. \end{cases} \tag{33}$$

By substituting Eqs. (25), (28), (30), (32) and (33) into Eq. (24) to reconstruct the potential energy of the drill-string system, the result is

$$\begin{aligned} V =& \frac{EA}{L_p}\left[(z_1 - V_0 t)^2 + (z_2 - z_1)^2\right] + \frac{GI_0}{L_p}\left[(\phi_1 - \phi_t)^2 + (\phi_2 - \phi_1)^2\right] \\ &+ \frac{24EI_x}{L_p^3}\left(x_1^2 + y_1^2\right) + m_1 g y_1. \end{aligned} \tag{34}$$

In order to describe the viscous damping influence of the drill-string system, the Rayleigh's dissipation function D is introduced and written as

$$D = \frac{1}{2}\left[c_a\left(\dot{z}_1^2 + \dot{z}_2^2\right) + c_b\left(\dot{x}_1^2 + \dot{y}_1^2\right) + c_t\left(\dot{\phi}_1^2 + \dot{\phi}_2^2\right)\right], \tag{35}$$

where c_a, c_b and c_t are the respective longitudinal, bending and torsional damping coefficients.

Then we apply Lagrange's Second Order Method, which can be expressed as follow

$$\frac{\mathrm{d}}{\mathrm{d}t}\left(\frac{\partial L}{\partial \dot{q}_i}\right) - \frac{\partial L}{\partial q_i} + \frac{\partial D}{\partial \dot{q}_i} = Q_{q_i}, \tag{36}$$

where $L = T - V$ is the Lagrange function. q_i (x_1, y_1, z_1, z_2, ϕ_1 and ϕ_2) are the generalized coordinates of the discrete system. Q_{q_i} denote the non-conservative generalized forces. By substituting Eqs. (23), (34) and (35) into Eq. (36), we obtain the equations of motion as expressed by Eq. (2), in which k_a, k_b and k_t can be determined as follow

$$k_a = \frac{2EA}{L_p}, \quad k_t = \frac{2GI_0}{L_p}, \quad k_b = \frac{48EI_x}{L_p^3}. \tag{37}$$

Appendix B. Numerical Algorithm

As can be seen from Eq. (2), the motions of the horizontal drill-string system are governed by 6 second-order differential equations, which can be reduced to 12 first-order differential equations of the below form

$$\mathbf{M}\dot{\mathbf{x}}\left(t\right) = \mathbf{b}\left(t\right) \tag{38}$$

where $\mathbf{x} = \left(\dot{x}_1, x_1, \dot{y}_1, y_1, \dot{z}_1, z_1, \dot{\phi}_1, \phi_1, \dot{z}_2, z_2, \dot{\phi}_2, \phi_2\right)$ is a state-space vector containing the longitudinal, lateral and angular displacements and velocities of the drill-string system. In order to balance the calculation speed and accuracy, the equations of motion are solved by using a Euler-forward finite difference technique [25, 34]. The solution procedure is advanced from time t to the next time step $t + \Delta t$ (Δt is the time increment) following the three steps listed below.

(i) The new solution values of the state-space vector $\mathbf{x}$ are computed from $\mathbf{x}\left(t + \Delta t\right) = \mathbf{x}\left(t\right) + \mathbf{M}^{-1}\mathbf{b}\left(t\right)\Delta t$.

(ii) The state-dependent time delay $t_n\left(t\right)$ is calculated from Eq. (13) by an inverse interpolation among two discrete $\phi_2\left(t\right)$.

(iii) The instantaneous depth of cut $d_N(t)$ is determined from Eq. (12). Similarly, $z_2(t - t_n(t))$ is linearly interpolated between two discrete $z_2(t)$.

Due to the existence of various motion regimes, including normal cutting, stick-slip and bit bounce, a relatively small time increment ($\Delta t = 10^{-5}10^{-4}$ s) should be adopted to acquire more accurate transition features between different regimes.

References

[1] Helms L. Horizontal drilling. *DMR Newsletter 2012*; 35(1): 1-3.

[2] Liu X, Vlajic N, Long X, Meng G, Balachandran B. Coupled axial-torsional dynamics in rotary drilling with state-dependent delay: stability and control. *Nonlinear Dyn 2014*; 78(3): 1891-1906.

[3] Sarker M, Rideout DG, Butt SD. Dynamic model for longitudinal and torsional motions of a horizontal oilwell drillstring with wellbore stick-slip friction. *J Petrol Sci Eng 2017*; 150: 272-287.

[4] Kovalyshen Y. Understanding root cause of stick-slip vibrations in deep drilling with drag bits. *Int J Non-Linear Mech 2014*; 67: 331-341.

[5] Dong G, Chen P. A review of the evaluation, control, and application technologies for drill String vibrations and shocks in oil and gas well. *Shock Vib 2016*; 2016: 1-34.

[6] Xue Q, Leung H, Wang R, Liu B, Huang L, Guo S. The chaotic dynamics of drilling. *Nonlinear Dyn 2015*; 83(4): 1-16.

[7] Ghasemloonia A, Geoff Rideout D, Butt SD. A review of drillstring vibration modeling and suppression methods. *J Petrol Sci Eng 2015*; 131: 150-164.

[8] Li Z, Zhang C, Song G. Research advances and debates on tubular mechanics in oil and gas wells. *J Petrol Sci Eng 2017*; 151: 194-212.

[9] Liao C-M, Vlajic N, Karki H, Balachandran B. Parametric studies on drill-string motions. *Int J Mech Sci 2012*; 54(1): 260-268.

[10] Melakhessou H, Berlioz A, Ferraris G. A nonlinear well-drillstring interaction model. *ASME J Vib Acoust 2003*; 125(1): 46-52.

[11] Liu X, Vlajic N, Long X, Meng G, Balachandran B. Nonlinear motions of a flexible rotor with a drill bit: stick-slip and delay effects. *Nonlinear Dyn 2013*; 72(1-2): 61-77.

[12] Zhu X, Li B, Liu Q, Chang X, Li L, Zhu K, Xu X. New analysis theory and method for drag and torque based on full-hole system dynamics in highly deviated well. *Math Probl Eng 2015*; 2015: 1-13.

[13] Tran QT, Nguyen KL, Manin L, Andrianoely MA, Dufour R, Mahjoub M, Menand S. Nonlinear dynamics of directional drilling with fluid and borehole interactions. *J Sound Vib 2019*; 462: 114924.

[14] de Moraes LPP, Savi Marcelo A. Drill-string vibration analysis considering an axial-torsional-lateral nonsmooth model. *J Sound Vib 2019*; 438: 220-237.

[15] Kapitaniak M, Vaziri V, Paez Chavez J, Wiercigroch M. Experimental studies of forward and backward whirls of drill-string. *Mech Syst Signal Pr 2018*; 100: 454-465.

[16] Tian J, Yang Y, Yang L. Vibration characteristics analysis and experimental study of horizontal drill string with wellbore random friction force. *Arch Appl Mech 2017*; 87: 1439-1451.

[17] Lian Z, Zhang Q, Lin T, Wang F. Experimental and numerical study of drill string dynamics in gas drilling of horizontal wells. *J Nat Gas Sci Eng 2015*; 27: 1412-1420.

[18] Lin T, Zhang Q, Lian Z, Xiao Z, Wang T, Li G, Ding J. Experimental study on vibrational behaviors of horizontal drillstring. *J Petrol Sci Eng 2018*; 164: 311-319.

[19] Ritto T, Escalante M, Sampaio R, Rosales M. Drill-string horizontal dynamics with uncertainty on the frictional force. *J Sound Vib 2013*; 332(1): 145-153.

[20] Cunha Jr. A, Soize C, Sampaio R. Computational modeling of the nonlinear stochastic dynamics of horizontal drillstrings. *Comput Mech 2015*; 56(5): 849-879.

[21] Wilson JK, Heisig G. Investigating the benefits of induced vibrations in unconventional horizontals via nonlinear drill string dynamics modeling. In *SPE/IADC drilling conference and exhibition*. SPE 173049-MS, 2015.

[22] Liu Y, Gao D. A nonlinear dynamic model for characterizing downhole motions of drill-string in a deviated well. *J Nat Gas Sci Eng 2017*; 38: 466-474.

[23] Han Y, Ai Z, Kuang Y, Liu J, Yan W. Nonlinear dynamic modeling of drill string in horizontal well - A geometrically exact approach. *J Petrol Sci Eng 2019*; 172: 1133-1152.

[24] Navarro-Lopez EM. An alternative characterization of bit-sticking phenomena in a multi-degree-of-freedom controlled drillstring. *Nonlinear Anal-Real 2009*; 10(5): 3162-3174.

[25] Germay C, Denoel V, Detournay E. Multiple mode analysis of the self-excited vibrations of rotary drilling systems. *J Sound Vib 2009*; 325(1): 362-381.

[26] Nandakumar K, Wiercigroch M. Stability analysis of a state dependent delayed, coupled two DOF model of drill-string vibration. *J Sound Vib 2013*; 332(10): 2575-2592.

[27] Yan Y, Wiercigroch M. Dynamics of rotary drilling with non-uniformly distributed blades. *Int J Mech Sci 2019*; 160: 270-281.

[28] Cheng Z, Jiang W, Ren G, Zhou J, Jiang S, Yang C, He B. A multibody dynamical model of full-hole drillstring system. *Acta Petrol Sin 2013*; 34(4): 753-758.

[29] Wang X. Finite Element Method. *Tsinghua University Press*; 2003.

[30] Huang K, Ai Z, Yang Y, Xie Z. The improved rock breaking efficiency of an annular-groove PDC bit. *J Petrol Sci Eng 2019*; 172: 425-435.

[31] Germay C, van de Wouw, Nijmeijer H, Sepulchre R. Nonlinear Drillstring Dynamics Analysis. *SIAM J Appl Dyn Syst 2009*; 8(2): 527-553.

[32] Kamel JM, Yigit AS. Modeling and analysis of stick-slip and bit bounce in oil well drillstrings equipped with drag bits. *J Sound Vib 2014*; 333(25): 6885-6899.

[33] Detournay E, Defourny P. A phenomenological model for the drilling action of drag bits. *Int J Rock Mech Min Sci 1992*; 29(1): 13-23.

[34] Richard T, Germay C, Detournay E. A simplified model to explore the root cause of stick-slip vibrations in drilling systems with drag bits. *J Sound Vib 2007*; 305(3): 432-456.

[35] Xue Q, Leung H, Huang L, Zhang R, Liu B, Wang J, Li L. Modeling of torsional oscillation of drillstring dynamics. *Nonlinear Dyn 2019*; 96(1): 267-283.

[36] Huang Z, Xie D, Xie B, Zhang W, Zhang F, He L. Investigation of PDC bit failure base on stick-slip vibration analysis of drilling string system plus drill bit. *J Sound Vib 2018*; 417: 97-109.

[37] Insperger T, Stepan G, Turi J. State-dependent delay in regenerative turning processes. *Nonlinear Dyn 2007*; 47(1-3): 275-283.

[38] Yan Y, Xu J, Wiercigroch M. Regenerative and frictional chatter in plunge grinding. *Nonlinear Dyn 2016*; 86(1): 283-307.

[39] Yan Y, Xu J, Wiercigroch M. Modelling of regenerative and frictional cutting dynamics. *Int J Mech Sci 2019*; 156: 86-93.